Modern Physics Letters A
Vol. 39, No. 9 (2024) 2450031 (11 pages)

DOI: 10.1142/S0217732324500317

World Scientific
www.worldscientific.com

Localized wave solutions to coupled variable-coefficient fourth-order nonlinear Schrödinger equations

N. Song[*,†], M. M. Guo and R. Liu

Department of Mathematics,
North University of China, Taiyuan,
Shanxi 030051, P. R. China
[*]*songni@nuc.edu.cn*

W. X. Ma[†]

Department of Mathematics,
Zhejiang Normal University, Jinhua,
Zhejiang 321004, P. R. China

Department of Mathematics,
King Abdulaziz University,
Jeddah 21589, Saudi Arabia

Department of Mathematics and Statistics,
University of South Florida,
Tampa, FL 33620-5700, USA

School of Mathematical and Statistical Sciences,
North-West University, Mafikeng Campus,
Private Bag X2046, Mmabatho 2735, South Africa
mawx@cas.usf.edu

Received 15 May 2023
Revised 21 August 2023
Accepted 28 February 2024
Published 5 April 2024

This study investigates higher-order localized waves for coupled variable-coefficient fourth-order nonlinear Schrödinger equations, which are used to describe the simultaneous propagation of optical pulses in an inhomogeneous optical fiber. Based on the seed solutions and Lax pair, the *N*th-order localized wave solutions are constructed. The interactions of rogue waves with dark–bright solitons are graphically analyzed via numerical simulation. The results are helpful for studying localized wave phenomena in nonlinear optics.

Keywords: Coupled variable-coefficient fourth-order nonlinear Schrödinger equations; generalized Darboux transformation; localized wave solution.

[†]Corresponding authors.

1. Introduction

It is well known that nonlinear science is fundamental to understanding many natural phenomena.[1–5] In recent years, with the advancement of modern science and technology, increasingly more scholars have focused on the dynamics of nonlinear evolution equations, which have been confirmed to describe many nonlinear phenomena.[3,6–9] In addition, the nonlinear evolution equations have been used to describe the propagation of multiple waves in nonlinear optical fibers, such as in optics,[10] oceanography,[11] Bose–Einstein condensates, etc.[12,13] However, when considering inhomogeneous optical fibers, variable-coefficient nonlinear Schrödinger (NLS) equations are considered to be more precise than constant-coefficient ones.[13–15] With heightened attention from scholars, variable-coefficient equations have been widely used to describe solitons, breathers, and rogue waves.[16,17]

Propagation of the ultrashort pulses in a long-distance and high-speed optical fiber transmission system can be governed by the fourth-order NLS equation. For the higher-order effects on optical fibers, the following coupled variable-coefficient fourth-order NLS equation is investigated. This equation is applied to describe the simultaneous propagation of nonlinear waves in an inhomogeneous optical fiber[18,19]:

$$\begin{aligned} iq_{j,t} &+ \sigma(t)q_{j,xx} + \mu(t)q_j\sum_{l=1}^{2}|q_l|^2 + \gamma_1(t)q_{1xxxx} + \gamma_2(t)q_j\sum_{l=1}^{2}|q_{l,x}|^2 + \gamma_3(t)q_{j,x} \\ &\times \sum_{l=1}^{2} q_l q_{l,x}^* + \gamma_4(t)q_{j,x}\sum_{l=1}^{2} q_l^* q_{l,x} + \gamma_5(t)q_{j,xx}\sum_{l=1}^{2}|q_l|^2 + \gamma_6(t)q_j\sum_{l=1}^{2} q_l^* q_{l,xx} \\ &+ \gamma_7(t)q_j\sum_{l=1}^{2} q_l q_{l,xx}^* + \gamma_8(t)q_j\left(\sum_{l=1}^{2}|q_l|^2\right)^2 = 0 \quad (j=1,2), \end{aligned} \tag{1}$$

where $q_1(x,t)$ and $q_2(x,t)$ represent the complex envelopes of two field polarization components, the subscript x indicates the partial derivatives with respect to the normalized propagation distance, and t represents the retarded time. Moreover, $\sigma(t)$ denotes the group velocity dispersion (GVD) coefficient, $\mu(t)$ is related to the self-phase modulation (SPM) coefficient, $\gamma_1(t)$ is the fourth-order dispersion coefficient, $\gamma_\alpha(t)$ $(\alpha = 2,\ldots,7)$ denotes the cubic nonlinear coefficients, $\gamma_8(t)$ is the quintic nonlinear coefficient, and $*$ represents the complex conjugate.

Several studies have been conducted on Eq. (1). For instance, Wang *et al.*[20] derived the two- and three-soliton solutions and graphically displayed the elastic and inelastic interactions. Lan[21] obtained the Lax pair and gave three different types of rogue waves. Xu *et al.*[22] obtained the soliton solutions via the Riemann–Hilbert method, and analyzed the dynamic behaviors of the one- and two-soliton solutions. Zhou *et al.*[23] investigated the vector breather waves and higher-order rogue waves via the Darboux-dressing transformation.

However, the localized waves for Eq. (1) have not been discussed. In this study, the localized wave solutions are obtained via the generalized Darboux transformation, and the dynamic characteristics are discussed via numerical simulation.

The remainder of this paper is prepared as follows. In Sec. 2, the generalized Darboux transformation is constructed, and the higher-order localized wave solutions are derived. In Sec. 3, via numerical simulation, the evolution plots of the higher-order localized waves are obtained, and the interactions between them are graphically analyzed. The conclusion is provided in Sec. 4.

2. Generalized Darboux Transformation

In this section, the following Lax pair of Eq. (1) is considered [20]:

$$\Phi_x = U\Phi, \tag{2a}$$

$$\Phi_t = V\Phi, \tag{2b}$$

where

$$U = \begin{pmatrix} -i\lambda & q_1 & q_2 \\ -q_1^* & i\lambda & 0 \\ -q_2^* & 0 & i\lambda \end{pmatrix}, \quad V = \begin{pmatrix} v_{11} & v_{12} & v_{13} \\ v_{21} & v_{22} & v_{23} \\ v_{31} & v_{32} & v_{33} \end{pmatrix},$$

$$\begin{aligned}
V_{11} &= 8i\gamma_1(t)\lambda^4 - 2i\left[\sigma(t) + 2\gamma_1(t)\sum_{l=1}^{2}|q_l|^2\right]\lambda^2 + 2\gamma_1(t)\sum_{l=1}^{2}(q_l^* q_{l,x} - q_l q_{l,x}^*)\lambda \\
&\quad - i\gamma_1(t)\left[\sum_{l=1}^{2}|q_{l,x}|^2 - \sum_{l=1}^{2}(q_l^* q_{l,xx} + q_l q_{l,xx}^*) - 3\left(\sum_{l=1}^{2}|q_l|^2\right)^2\right] + i\sigma(t)\sum_{l=1}^{2}|q_l|^2, \\
V_{1,s} &= -8\gamma_1(t)q_{s-1}\lambda^3 - 4iq_{s-1,x}\lambda^2 + 2\left[\sigma(t)q_{s-1} + \gamma_1(t)q_{s-1,xx} + 2\gamma_1(t)q_{s-1}\sum_{l=1}^{2}\right. \\
&\quad \left.\times|q_l|^2\right]\lambda + i\gamma_1(t)\left[q_{s-1,xxx} + 3q_{s-1,x}\sum_{l=1}^{2}|q_l|^2 + 3q_{s-1,x}\sum_{l=1}^{2}q_l^* q_{l,x}\right] + i\sigma(t)q_{s-1,x}, \\
V_{1,s} &= -8\gamma_1(t)q_{s-1}\lambda^3 - 4iq_{s-1,x}\lambda^2 + 2\left[\sigma(t)q_{s-1} + \gamma_1(t)q_{s-1,xx} + 2\gamma_1(t)q_{s-1}\sum_{l=1}^{2}|q_l|^2\right] \\
&\quad \times\lambda + i\gamma_1(t)\left[q_{s-1,xxx} + 3q_{s-1,x}\sum_{l=1}^{2}|q_l|^2 + 3q_{s-1,x}\sum_{l=1}^{2}q_l^* q_{l,x}\right] + i\sigma(t)q_{s-1,x}, \\
V_{s,s} &= 8i\gamma_1(t)\lambda^4 + 2i[\sigma(t) + 2\gamma_1(t)|q_{s-1}|^2]\lambda^2 + 2\gamma_1(t)(q_{s-1}q_{s-1,x}^* - q_{s-1}^* q_{s-1,x})\lambda \\
&\quad - 3i\gamma_1(t)|q_{s-1}|^2\sum_{l=1}^{2}|q_l|^2 + i\gamma_1(t)[|q_{s-1,x}|^2 - q_{s-1}q_{s-1,xx}^* - q_{s-1}^* q_{s-1,xx}] \\
&\quad - i\sigma(t)|q_{s-1}|^2, \\
V_{23} &= 4i\gamma_1(t)q_1^* q_2\lambda^2 + 2\gamma_1(t)(q_{1,x}^* q_2 - q_1^* q_{2,x})\lambda - 3i\gamma_1(t)q_1^* q_2\sum_{l=1}^{2}|q_l|^2 \\
&\quad + i\gamma_1(t)(q_{2,x}q_{1,x}^* - q_1^* q_{2,xx} - q_{1,xx}^* q_2) - i\sigma(t)q_1^* q_2, \\
V_{32} &= -V_{23}^*, \quad V_{s,1} = -V_{1,s}^*.
\end{aligned}$$

It can be verified that the compatibility condition $U_t - V_x + UV - VU = 0$ is equivalent to Eq. (1) under the constraints

$$\mu(t) = 2\sigma(t), \quad \gamma_2(t) = 2\gamma_1(t), \quad \gamma_3(t) = 2\gamma_1(t), \quad \gamma_4(t) = 6\gamma_1(t),$$
$$\gamma_5(t) = 4\gamma_1(t), \quad \gamma_6(t) = 4\gamma_1(t), \quad \gamma_7(t) = 2\gamma_1(t), \quad \gamma_8(t) = 6\gamma_1(t).$$

The generalized Darboux transformation of Eq. (1) can be constructed as follows:

$$\Phi_1 = \Phi_1^{[0]} + \Phi_1^{[1]}\eta + \Phi_1^{[2]}\eta^2 + \cdots + \Phi_1^{[N]}\eta^N + o(\eta^N), \tag{3}$$

where

$$\Phi_1^k = \frac{1}{k!}\frac{\partial^k}{\partial\lambda^k}\Phi_1(\lambda)\bigg|_{\lambda=\lambda_1} = (\phi_1^{[k]}, \varphi_1^{[k]}, \chi_1^{[k]})^T \quad (k = 0, 1, 2, \ldots, N). \tag{4}$$

Therefore, the generalized Darboux transformation is defined as follows:

$$q_1[N] = q_1[N-1] - 2i(\lambda_1 - \lambda_1^*)\frac{\phi_1[N-1]\varphi_1^*[N-1]}{|\phi_1[N-1]|^2 + |\varphi_1[N-1]|^2 + |\chi_1[N-1]|^2}, \tag{5a}$$

$$q_2[N] = q_2[N-1] - 2i(\lambda_1 - \lambda_1^*)\frac{\phi_1[N-1]\chi_1^*[N-1]}{|\phi_1[N-1]|^2 + |\varphi_1[N-1]|^2 + |\chi_1[N-1]|^2}. \tag{5b}$$

3. Localized Wave Solutions for Eq. (1)

To construct the localized wave solutions for Eq. (1), consider the seed solutions $q_1^{[0]} = a_1 e^{i\theta(t)}$ and $q_2^{[0]} = a_2 e^{i\theta(t)}$ with $\theta(t) = \int 2\sigma(t)(a_1^2 + a_2^2) + 6\gamma(t)(a_1^2 + a_2^2)^2 dt$, where a_1 and a_2 are the real constants. The corresponding basic vector solution at $\lambda = (i\sqrt{a_1^2 + a_2^2})(1 + \eta^2)$ is as follows:

$$\Phi_1(\eta) = \begin{pmatrix} (C_1 e^{M_1+M_2} - C_2 e^{M_1-M_2})e^{\frac{i\omega(t)}{2}} \\ \rho_1(C_1 e^{M_1-M_2} - C_2 e^{M_1+M_2})e^{-\frac{i\omega(t)}{2}} + \varpi a_2 e^{M_3} \\ \rho_2(C_1 e^{M_1-M_2} - C_2 e^{M_1+M_2})e^{-\frac{i\omega(t)}{2}} - \varpi a_1 e^{M_3} \end{pmatrix}, \tag{6}$$

where

$$C_1 = \frac{\sqrt{\lambda - \sqrt{\lambda^2 + a_1^2 + a_2^2}}}{\sqrt{\lambda^2 + a_1^2 + a_2^2}}, \quad C_2 = \frac{\sqrt{\lambda + \sqrt{\lambda^2 + a_1^2 + a_2^2}}}{\sqrt{\lambda^2 + a_1^2 + a_2^2}},$$

$$M_1 = 0, \quad M_2 = i\sqrt{\lambda^2 + a_1^2 + a_2^2}(x - 4\gamma(t)\lambda^3 t + \lambda t(\sigma(t) + 2\gamma(t)(a_1^2 + a_2^2) + \Omega(\eta))),$$

$$M_3 = i\lambda x + (-8i\gamma(t)\lambda^4 + 2i\sigma(t)\lambda^2)t, \quad \rho_1 = \frac{a_1}{\sqrt{a_1^2 + a_2^2}},$$

$$\rho_2 = \frac{a_2}{\sqrt{a_1^2 + a_2^2}}, \quad \Omega(\eta) = \sum_{j=1}^{N}(m_j + in_j)\eta^{2j},$$

and ϖ, m_j, and n_j are arbitrary real constants.

The different expressions of the coefficients can generate certain structures related to the pulse propagation. In this section, the dynamics of the first-order localized waves are discussed.

Considering Eqs. (5a) and (5b), when $N = 1$, Fig. 1(a) exhibits the interactions between the first-order rogue waves and the dark solitons, which have a constant

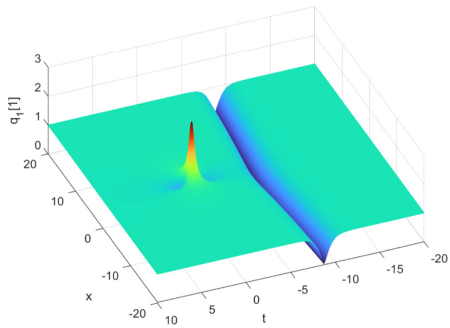

(a)

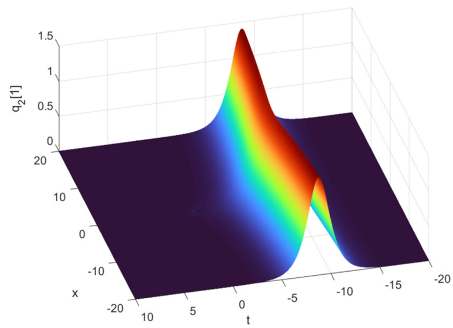

(d)

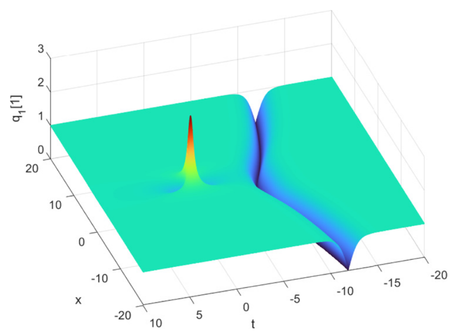

(b)

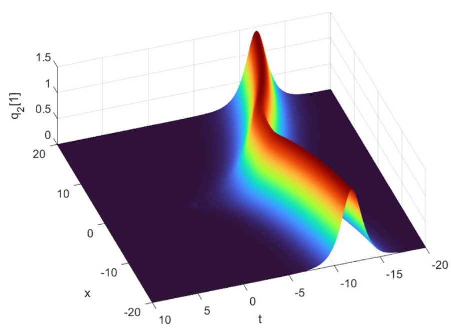

(e)

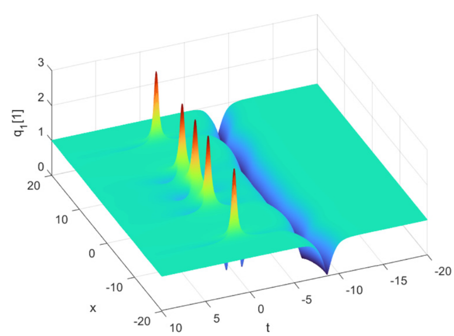

(c)

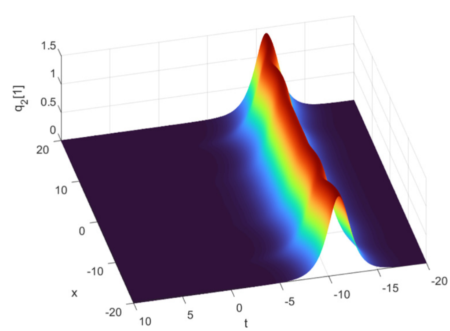

(f)

Fig. 1. The first-order localized waves with $a_1 = 1$, $a_2 = 0$, and $\varpi = \frac{1}{100}$: (a), (d) $\sigma(t) = 1$, $\gamma_1(t) = 0$; (b), (e) $\sigma(t) = 1$, $\gamma_1(t) = \frac{t^2}{100}$; (c), (f) $\sigma(t) = \cos(\frac{t}{3})$, $\gamma_1(t) = 0$.

velocity, when parameters $\sigma(t)$ and $\gamma_1(t)$ are both constants. After changing the value of $\gamma_1(t)$ to a variable-coefficient, as shown in Fig. 1(b), the dark soliton is bent, and presents a "V" shape. When changing $\sigma(t)$ into a trigonometric function, periodic rogue waves interact with a dark soliton. Under the influence of a zero-amplitude background, the first-order rogue waves in the component $q_2[1]$ are not easily observed, as shown in Figs. 1(d)–1(f).

Figure 2 shows the interplay of the first-order rogue waves with a breather. Let $a_1 \neq 0$ and $a_2 \neq 0$, where a_1 and a_2 are both constants. When $\sigma(t)$ and $\gamma_1(t)$ are both constants and $\gamma_1(t) = 0$, which is as same as the situation presented in Fig. 1(a), the first-order rogue wave interacts with the periodic breather. Let $\sigma(t)$ be a trigonometric function, and the obtained evolutions of periodic rogue waves interacting with a breather are shown in Figs. 2(b) and 2(d). Moreover, it is evident that the amplitude of $q_2[1]$ is higher than that of $q_2[1]$.

Similarly, when $N = 2$, the dynamic characteristics of the second-order localized waves are discussed by altering the values of the free parameters a_1, a_2, $\sigma(t)$, and $\gamma_1(t)$.

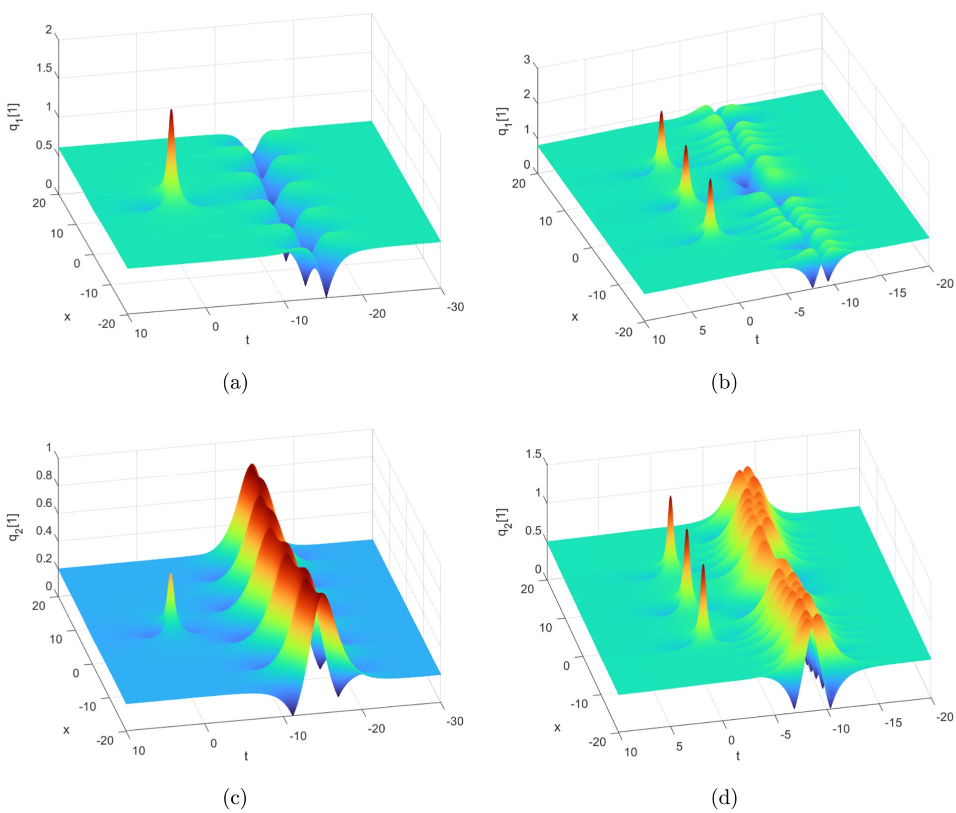

Fig. 2. The first-order localized waves with (a), (c) $a_1 = 0.6$, $a_2 = 0.2$, $\sigma(t) = 1$, and $\gamma_1(t) = 0$; (b), (d) $a_1 = 0.8$, $a_2 = 0.5$, $\sigma(t) = \cos(\frac{t}{5})$, and $\gamma_1(t) = 0$.

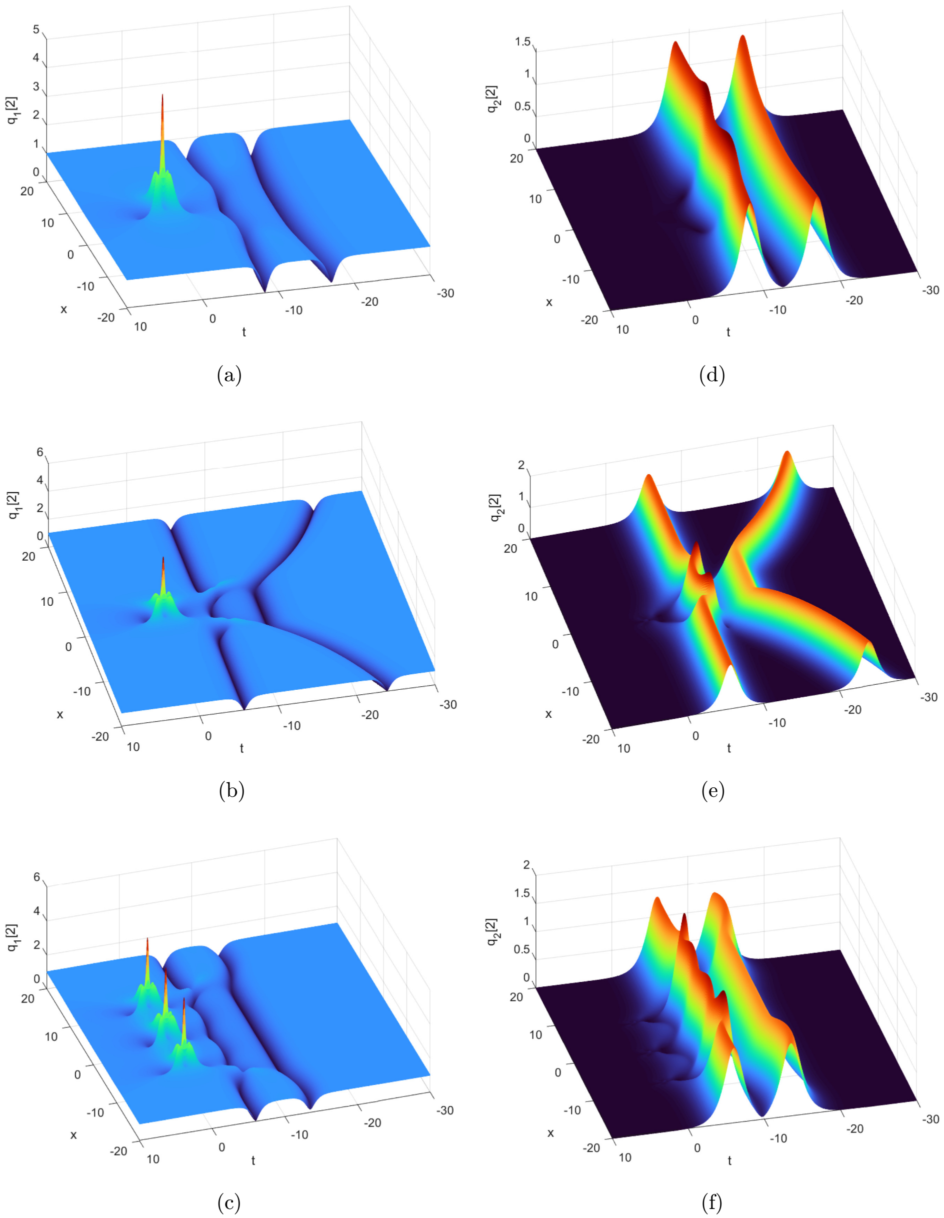

Fig. 3. The second-order localized waves with $a_1 = 1$, $a_2 = 0$, and $\varpi = \frac{1}{100}$: (a), (d) $\sigma(t) = 1$, $\gamma_1(t) = 0$; (b), (e) $\sigma(t) = 1$, $\gamma_1(t) = \frac{t^2}{100}$; (c), (f) $\sigma(t) = \cos(\frac{t}{5})$, $\gamma_1(t) = 0$.

The interactions between the second-order rogue waves and dark–bright solitons are depicted in Fig. 3. Let $\sigma(t)$ and $\gamma_1(t)$ be constants, the values of which are the same as those presented in Fig. 1(a). Figure 3(a) displays the evolution of the second-order rogue waves interacting with two dark solitons. By increasing the value of

$\gamma_1(t)$, the second-order rogue waves interact with the K-shaped dark–bright solitons, as shown in Figs. 3(b) and 3(e). By changing the value of $\sigma(t)$ to a trigonometric function, three second-order rogue waves interact with the dark–bright solitons.

Figure 4 presents the interplay of the second-order rogue waves with the dark–bright solitons. Different from Fig. 3, when $m_1 = 10$ and $n_1 = 10$, Fig. 4 reveals

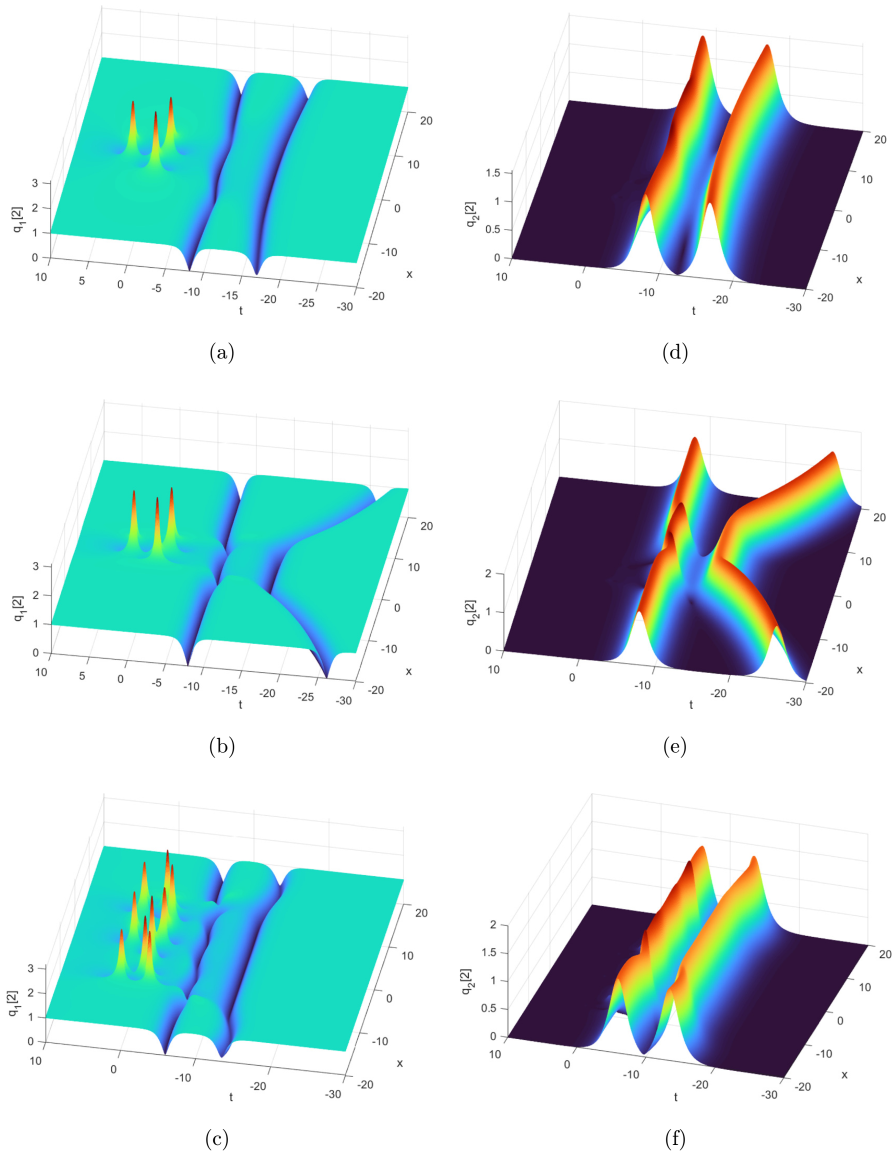

Fig. 4. The second-order localized waves with $a_1 = 1$, $a_2 = 0$, and $\varpi = \frac{1}{100}$: (a), (d) $\sigma(t) = 1$, $\gamma_1(t) = 0$, $m_1 = 10$, and $n_1 = 10$; (b), (e) $\sigma(t) = 1$, $\gamma_1(t) = \frac{t^2}{100}$, $m_1 = 10$, and $n_1 = 10$; (c), (f) $\sigma(t) = \cos(\frac{t}{5})$, $\gamma_1(t) = 0$, $m_1 = 5$, and $n_1 = 5$.

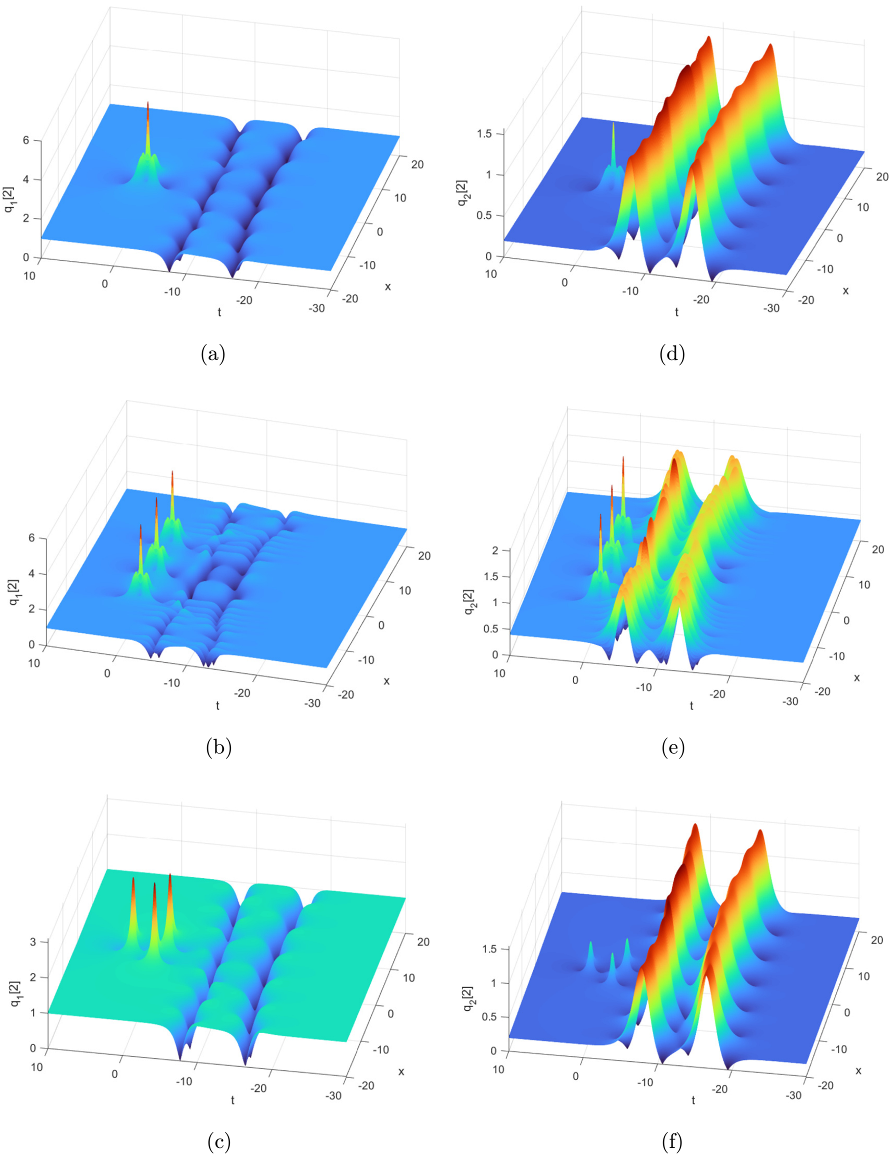

Fig. 5. The second-order localized waves with (a), (d) $a_1 = 1$, $a_2 = 0.2$, $\sigma(t) = 1$, $\gamma_1(t) = 0$, $m_1 = 0$, and $n_1 = 0$; (b), (e) $a_1 = 1$, $a_2 = 0.4$, $\sigma(t) = 1$, $\gamma_1(t) = \frac{t^2}{100}$, $m_1 = 0$, and $n_1 = 0$; (c), (f) $a_1 = 1$, $a_2 = 0.2$, $\sigma(t) = 1$, $\gamma_1(t) = 0$, $m_1 = 10$, and $n_1 = 10$.

that the second-order rogue waves are separated into three first-order rogue waves that form a triangular structure. It is difficult to observe the rogue waves in the component $q_2[2]$ due to the zero-amplitude background.

Let $a_1 \neq 0$ and $a_2 \neq 0$. Figure 5 displays the dynamics of the second-order rogue waves and breathers. Based on the parameters, the periods of the breathers decrease with the increase of the value of $\sigma(t)$. Figures 5(c) and 5(f) reveal that the second-order rogue waves are split into three first-order rogue waves. In addition, Fig. 5 shows that the amplitude of $q_1[2]$ is lower than that of $q_2[2]$.

4. Conclusion

This study investigated the coupled variable-coefficient fourth-order NLS equation, which describes the simultaneous propagation of nonlinear waves in an inhomogeneous optical fiber. Via Taylor expansion and the limit formula, the generalized Darboux transformation was constructed. Based on the seed solutions and the Lax pair, the first- and second-order localized solutions were given. There are several free parameters, namely a_1, a_2, $\sigma(t)$, and $\gamma_1(t)$, that influence the propagation shape of the localized waves. The effects of these parameters for Eq. (1) were graphically analyzed.

Parameters a_1 and a_2 determine the type of localized waves. The interaction between the rogue waves and the dark–bright solitons when $a_1 \neq 0$ and $a_2 = 0$ was presented, as was the propagation of the rogue waves and the breathers when $a_1 \neq 0$ and $a_2 \neq 0$. Furthermore, the variable-coefficient $\gamma_1(t)$ was found to affect the shapes of the solitons, the propagation direction of the solitons was parallel to the x-axis when $\gamma_1(t) = 0$. Besides, the shape of the solitons became bend as the increase of the value of $\gamma_1(t)$. Rogue waves with periodicity were revealed when the variable-coefficient $\sigma(t)$ is a trigonometric function, and the periods of the rogue waves were found to decrease with the decrease of the period of $\sigma(t)$. Parameters m_1 and n_1 influence the separation of the second-order rogue waves. When $m_1 \cdot n_1 \neq 0 (i = 1, 2)$, the second-order rogue wave can be divided into three first-order rogue waves. The authors hope that the results will help to understand the localized waves phenomena in nonlinear optics, and can be verified in the future experiments.

Acknowledgments

The authors sincerely thank the support offered by the National Natural Science Foundation of China (NNSFC) through Grant Nos. 11602232 and 12372026, the Shanxi Natural Science Foundation (SNSF) through Grant Nos. 202203021211086 and 202203021211088, the Shanxi Province Research Funding Program for Returning Students (2022-150), and the Natural Science Foundation of Inner Mongolia Autonomous Region through Grant No. 2019LH01002.

ORCID

N. Song https://orcid.org/0000-0002-0629-7015
M. M. Guo https://orcid.org/0009-0005-5899-4276
R. Liu https://orcid.org/0009-0006-3923-1457
W. X. Ma https://orcid.org/0000-0001-5309-1493

References

1. A. Tripathy *et al.*, *Optik* **281**, 170817 (2023).
2. D. Yang, *J. Math. Anal. Appl.* **519**, 126764 (2023).
3. Y. Yang, T. Wang and H. Guo, *J. Math. Anal. Appl.* **520**, 126877 (2023).
4. C. C. Ding *et al.*, *Opt. Express* **30**, 40712 (2022).
5. N. Song, Y. Lei and D. Cao, *Acta Mech. Sin.* **38**, 521500 (2022).
6. H. Rezazadeh *et al.*, *Results Phys.* **49**, 106452 (2023).
7. P. K. Das *et al.*, *Optik* **283**, 170888 (2023).
8. T. Mathanaranjan, *J. Nonlinear Opt. Phys. Mater.* **32**, 2350016 (2023).
9. Y. H. Yin, X. Lü and W. X. Ma, *Nonlinear Dyn.* **108**, 4181 (2022).
10. R. R. Jia and Y. F. Wang, *Wave Motion* **114**, 103042 (2022).
11. H. Wang and Y. Zhang, *J. Comput. Appl. Math.* **420**, 114812 (2023).
12. C. C. Ding *et al.*, *Chaos Solitons Fractals* **169**, 113247 (2023).
13. C. C. Ding *et al.*, *Chin. Phys. Lett.* **40**, 040501 (2023).
14. R. M. El-Shiekh, *Results Phys.* **13**, 102214 (2019).
15. M. S. Osman *et al.*, *J. Ocean Eng. Sci.* **7**, 431 (2022).
16. Z. Zhang *et al.*, *Eur. Phys. J. Plus* **134**, 1 (2019).
17. N. Song *et al.*, *Nonlinear Dyn.* **111**, 5709 (2023).
18. A. Degasperis and S. Lombardo, *Phys. Rev. E* **88**, 052914 (2013).
19. Z. Du *et al.*, *Eur. Phys. J. Plus* **135**, 1 (2020).
20. M. Wang *et al.*, *Appl. Math. Lett.* **119**, 106936 (2021).
21. Z. Z. Lan, *Appl. Math. Lett.* **98**, 128 (2019).
22. T. Y. Xu, S. F. Tian and W. Q. Peng, *Math. Methods Appl. Sci.* **43**, 865 (2020).
23. X. M. Zhou *et al.*, *Int. J. Comput. Math.* **98**, 2504 (2021).